

Improved measurement of the branching fraction of $D_s^+ \rightarrow \mu^+ \nu_\mu$

M. Ablikim,¹ M. N. Achasov,^{13,b} P. Adlarson,⁷⁵ X. C. Ai,⁸¹ R. Aliberti,³⁶ A. Amoroso,^{74a,74c} M. R. An,⁴⁰ Q. An,^{71,58} Y. Bai,⁵⁷ O. Bakina,³⁷ I. Balossino,^{30a} Y. Ban,^{47,g} V. Batozskaya,^{1,45} K. Begzsuren,³³ N. Berger,³⁶ M. Berlowski,⁴⁵ M. Bertani,^{29a} D. Bettoni,^{30a} F. Bianchi,^{74a,74c} E. Bianco,^{74a,74c} J. Bloms,⁶⁸ A. Bortone,^{74a,74c} I. Boyko,³⁷ R. A. Briere,⁵ A. Brueggemann,⁶⁸ H. Cai,⁷⁶ X. Cai,^{1,58} A. Calcaterra,^{29a} G. F. Cao,^{1,63} N. Cao,^{1,63} S. A. Cetin,^{62a} J. F. Chang,^{1,58} T. T. Chang,⁷⁷ W. L. Chang,^{1,63} G. R. Che,⁴⁴ G. Chelkov,^{37,a} C. Chen,⁴⁴ Chao Chen,⁵⁵ G. Chen,¹ H. S. Chen,^{1,63} M. L. Chen,^{1,58,63} S. J. Chen,⁴³ S. M. Chen,⁶¹ T. Chen,^{1,63} X. R. Chen,^{32,63} X. T. Chen,^{1,63} Y. B. Chen,^{1,58} Y. Q. Chen,³⁵ Z. J. Chen,^{26,h} Z. Y. Chen,^{1,63} W. S. Cheng,^{74c} S. K. Choi,^{10a} X. Chu,⁴⁴ G. Cibinetto,^{30a} S. C. Coen,⁴ F. Cossio,^{74c} J. J. Cui,⁵⁰ H. L. Dai,^{1,58} J. P. Dai,⁷⁹ A. Dbeysi,¹⁹ R. E. de Boer,⁴ D. Dedovich,³⁷ Z. Y. Deng,¹ A. Denig,³⁶ I. Denysenko,³⁷ M. Destefanis,^{74a,74c} F. De Mori,^{74a,74c} B. Ding,^{66,1} X. X. Ding,^{47,g} Y. Ding,⁴¹ Y. Ding,³⁵ J. Dong,^{1,58} L. Y. Dong,^{1,63} M. Y. Dong,^{1,58,63} X. Dong,⁷⁶ S. X. Du,⁸¹ Z. H. Duan,⁴³ P. Egorov,^{37,a} Y. L. Fan,⁷⁶ J. Fang,^{1,58} S. S. Fang,^{1,63} W. X. Fang,¹ Y. Fang,¹ R. Farinelli,^{30a} L. Fava,^{74b,74c} F. Feldbauer,⁴ G. Felici,^{29a} C. Q. Feng,^{71,58} J. H. Feng,⁵⁹ K. Fischer,⁶⁹ M. Fritsch,⁴ C. Fritsch,⁶⁸ C. D. Fu,¹ J. L. Fu,⁶³ Y. W. Fu,¹ H. Gao,⁶³ Y. N. Gao,^{47,g} Yang Gao,^{71,58} S. Garbolino,^{74c} I. Garzia,^{30a,30b} P. T. Ge,⁷⁶ Z. W. Ge,⁴³ C. Geng,⁵⁹ E. M. Gersabeck,⁶⁷ A. Gilman,⁶⁹ K. Goetzen,¹⁴ L. Gong,⁴¹ W. X. Gong,^{1,58} W. Gradl,³⁶ S. Gramigna,^{30a,30b} M. Greco,^{74a,74c} M. H. Gu,^{1,58} Y. T. Gu,¹⁶ C. Y. Guan,^{1,63} Z. L. Guan,²³ A. Q. Guo,^{32,63} L. B. Guo,⁴² M. J. Guo,⁵⁰ R. P. Guo,⁴⁹ Y. P. Guo,^{12,f} A. Guskov,^{37,a} T. T. Han,⁵⁰ W. Y. Han,⁴⁰ X. Q. Hao,²⁰ F. A. Harris,⁶⁵ K. K. He,⁵⁵ K. L. He,^{1,63} F. H. H. Heinsius,⁴ C. H. Heinz,³⁶ Y. K. Heng,^{1,58,63} C. Herold,⁶⁰ T. Holtmann,⁴ P. C. Hong,^{12,f} G. Y. Hou,^{1,63} X. T. Hou,^{1,63} Y. R. Hou,⁶³ Z. L. Hou,¹ H. M. Hu,^{1,63} J. F. Hu,^{56,i} T. Hu,^{1,58,63} Y. Hu,¹ G. S. Huang,^{71,58} K. X. Huang,⁵⁹ L. Q. Huang,^{32,63} X. T. Huang,⁵⁰ Y. P. Huang,¹ T. Hussain,⁷³ N. Hüskens,^{28,36} W. Imoehl,²⁸ M. Irshad,^{71,58} J. Jackson,²⁸ S. Jaeger,⁴ S. Janchiv,³³ J. H. Jeong,^{10a} Q. Ji,¹ Q. P. Ji,²⁰ X. B. Ji,^{1,63} X. L. Ji,^{1,58} Y. Y. Ji,⁵⁰ X. Q. Jia,⁵⁰ Z. K. Jia,^{71,58} P. C. Jiang,^{47,g} S. S. Jiang,⁴⁰ T. J. Jiang,¹⁷ X. S. Jiang,^{1,58,63} Y. Jiang,⁶³ J. B. Jiao,⁵⁰ Z. Jiao,²⁴ S. Jin,⁴³ Y. Jin,⁶⁶ M. Q. Jing,^{1,63} T. Johansson,⁷⁵ X. K.,¹ S. Kabana,³⁴ N. Kalantar-Nayestanaki,⁶⁴ X. L. Kang,⁹ X. S. Kang,⁴¹ R. Kappert,⁶⁴ M. Kavatsyuk,⁶⁴ B. C. Ke,⁸¹ A. Khoukaz,⁶⁸ R. Kiuchi,¹ R. Kliemt,¹⁴ O. B. Kolcu,^{62a} B. Kopf,⁴ M. K. Kuessner,⁴ A. Kupsc,^{45,75} W. Kühn,³⁸ J. J. Lane,⁶⁷ P. Larin,¹⁹ A. Lavania,²⁷ L. Lavezzi,^{74a,74c} T. T. Lei,^{71,k} Z. H. Lei,^{71,58} H. Leithoff,³⁶ M. Lellmann,³⁶ T. Lenz,³⁶ C. Li,⁴⁸ C. Li,⁴⁴ C. H. Li,⁴⁰ Cheng Li,^{71,58} D. M. Li,⁸¹ F. Li,^{1,58} G. Li,¹ H. Li,^{71,58} H. B. Li,^{1,63} H. J. Li,²⁰ H. N. Li,^{56,i} Hui Li,⁴⁴ J. R. Li,⁶¹ J. S. Li,⁵⁹ J. W. Li,⁵⁰ K. L. Li,²⁰ Ke Li,¹ L. J. Li,^{1,63} L. K. Li,¹ Lei Li,³ M. H. Li,⁴⁴ P. R. Li,^{39,j,k} Q. X. Li,⁵⁰ S. X. Li,¹² T. Li,⁵⁰ W. D. Li,^{1,63} W. G. Li,¹ X. H. Li,^{71,58} X. L. Li,⁵⁰ Xiaoyu Li,^{1,63} Y. G. Li,^{47,g} Z. J. Li,⁵⁹ Z. X. Li,¹⁶ C. Liang,⁴³ H. Liang,^{1,63} H. Liang,^{71,58} H. Liang,³⁵ Y. F. Liang,⁵⁴ Y. T. Liang,^{32,63} G. R. Liao,¹⁵ L. Z. Liao,⁵⁰ J. Libby,²⁷ A. Limphirat,⁶⁰ D. X. Lin,^{32,63} T. Lin,¹ B. J. Liu,¹ B. X. Liu,⁷⁶ C. Liu,³⁵ C. X. Liu,¹ F. H. Liu,⁵³ Fang Liu,¹ Feng Liu,⁶ G. M. Liu,^{56,i} H. Liu,^{39,j,k} H. B. Liu,¹⁶ H. M. Liu,^{1,63} Huanhuan Liu,¹ Huihui Liu,²² J. B. Liu,^{71,58} J. L. Liu,⁷² J. Y. Liu,^{1,63} K. Liu,¹ K. Y. Liu,⁴¹ Ke Liu,²³ L. Liu,^{71,58} L. C. Liu,⁴⁴ Lu Liu,⁴⁴ M. H. Liu,^{12,f} P. L. Liu,¹ Q. Liu,⁶³ S. B. Liu,^{71,58} T. Liu,^{12,f} W. K. Liu,⁴⁴ W. M. Liu,^{71,58} X. Liu,^{39,j,k} Y. Liu,^{39,j,k} Y. Liu,⁸¹ Y. B. Liu,⁴⁴ Z. A. Liu,^{1,58,63} Z. Q. Liu,⁵⁰ X. C. Lou,^{1,58,63} F. X. Lu,⁵⁹ H. J. Lu,²⁴ J. G. Lu,^{1,58} X. L. Lu,¹ Y. Lu,⁷ Y. P. Lu,^{1,58} Z. H. Lu,^{1,63} C. L. Luo,⁴² M. X. Luo,⁸⁰ T. Luo,^{12,f} X. L. Luo,^{1,58} X. R. Lyu,⁶³ Y. F. Lyu,⁴⁴ F. C. Ma,⁴¹ H. L. Ma,¹ J. L. Ma,^{1,63} L. L. Ma,⁵⁰ M. M. Ma,^{1,63} Q. M. Ma,¹ R. Q. Ma,^{1,63} R. T. Ma,⁶³ X. Y. Ma,^{1,58} Y. Ma,^{47,g} Y. M. Ma,³² F. E. Maas,¹⁹ M. Maggiora,^{74a,74c} S. Malde,⁶⁹ A. Mangoni,^{29b} Y. J. Mao,^{47,g} Z. P. Mao,¹ S. Marcello,^{74a,74c} Z. X. Meng,⁶⁶ J. G. Messchendorp,^{14,64} G. Mezzadri,^{30a} H. Miao,^{1,63} T. J. Min,⁴³ R. E. Mitchell,²⁸ X. H. Mo,^{1,58,63} N. Yu. Muchnoi,^{13,b} Y. Nefedov,³⁷ F. Nerling,^{19,d} I. B. Nikolaev,^{13,b} Z. Ning,^{1,58} S. Nisar,^{11,1} Y. Niu,⁵⁰ S. L. Olsen,⁶³ Q. Ouyang,^{1,58,63} S. Pacetti,^{29b,29c} X. Pan,⁵⁵ Y. Pan,⁵⁷ A. Pathak,³⁵ P. Patteri,^{29a} Y. P. Pei,^{71,58} M. Pelizaeus,⁴ H. P. Peng,^{71,58} K. Peters,^{14,d} J. L. Ping,⁴² R. G. Ping,^{1,63} S. Plura,³⁶ S. Pogodin,³⁷ V. Prasad,³⁴ F. Z. Qi,¹ H. Qi,^{71,58} H. R. Qi,⁶¹ M. Qi,⁴³ T. Y. Qi,^{12,f} S. Qian,^{1,58} W. B. Qian,⁶³ C. F. Qiao,⁶³ J. J. Qin,⁷² L. Q. Qin,¹⁵ X. P. Qin,^{12,f} X. S. Qin,⁵⁰ Z. H. Qin,^{1,58} J. F. Qiu,¹ S. Q. Qu,⁶¹ C. F. Redmer,³⁶ K. J. Ren,⁴⁰ A. Rivetti,^{74c} V. Rodin,⁶⁴ M. Rolo,^{74c} G. Rong,^{1,63} Ch. Rosner,¹⁹ S. N. Ruan,⁴⁴ N. Salone,⁴⁵ A. Sarantsev,^{37,c} Y. Schelhaas,³⁶ K. Schoenning,⁷⁵ M. Scodreggio,^{30a,30b} K. Y. Shan,^{12,f} W. Shan,²⁵ X. Y. Shan,^{71,58} J. F. Shangguan,⁵⁵ L. G. Shao,^{1,63} M. Shao,^{71,58} C. P. Shen,^{12,f} H. F. Shen,^{1,63} W. H. Shen,⁶³ X. Y. Shen,^{1,63} B. A. Shi,⁶³ H. C. Shi,^{71,58} J. L. Shi,¹² J. Y. Shi,¹ Q. Q. Shi,⁵⁵ R. S. Shi,^{1,63} X. Shi,^{1,58} J. J. Song,²⁰ T. Z. Song,⁵⁹ W. M. Song,^{35,1} Y. J. Song,¹² Y. X. Song,^{47,g} S. Sosio,^{74a,74c} S. Spataro,^{74a,74c} F. Stieler,³⁶ Y. J. Su,⁶³ G. B. Sun,⁷⁶ G. X. Sun,¹ H. Sun,⁶³ H. K. Sun,¹ J. F. Sun,²⁰ K. Sun,⁶¹ L. Sun,⁷⁶ S. S. Sun,^{1,63} T. Sun,^{1,63} W. Y. Sun,³⁵ Y. Sun,⁹ Y. J. Sun,^{71,58} Y. Z. Sun,¹ Z. T. Sun,⁵⁰ Y. X. Tan,^{71,58} C. J. Tang,⁵⁴ G. Y. Tang,¹ J. Tang,⁵⁹ Y. A. Tang,⁷⁶ L. Y. Tao,⁷² Q. T. Tao,^{26,h} M. Tat,⁶⁹ J. X. Teng,^{71,58} V. Thoren,⁷⁵ W. H. Tian,⁵⁹ W. H. Tian,⁵² Y. Tian,^{32,63} Z. F. Tian,⁷⁶ I. Uman,^{62b} S. J. Wang,⁵⁰ B. Wang,¹ B. L. Wang,⁶³ Bo Wang,^{71,58} C. W. Wang,⁴³ D. Y. Wang,^{47,g} F. Wang,⁷² H. J. Wang,^{39,j,k} H. P. Wang,^{1,63} J. P. Wang,⁵⁰ K. Wang,^{1,58} L. L. Wang,¹ M. Wang,⁵⁰ Meng Wang,^{1,63} S. Wang,^{39,j,k} S. Wang,^{12,f} T. Wang,^{12,f} T. J. Wang,⁴⁴ W. Wang,⁵⁹ W. Wang,⁷² W. P. Wang,^{71,58} X. Wang,^{47,g} X. F. Wang,^{39,j,k} X. J. Wang,⁴⁰ X. L. Wang,^{12,f} Y. Wang,⁶¹ Y. D. Wang,⁴⁶ Y. F. Wang,^{1,58,63} Y. H. Wang,⁴⁸ Y. N. Wang,⁴⁶ Y. Q. Wang,¹

Yaqian Wang,^{18,1} Yi Wang,⁶¹ Z. Wang,^{1,58} Z. L. Wang,⁷² Z. Y. Wang,^{1,63} Ziyi Wang,⁶³ D. Wei,⁷⁰ D. H. Wei,¹⁵ F. Weidner,⁶⁸ S. P. Wen,¹ C. W. Wenzel,⁴ U. W. Wiedner,⁴ G. Wilkinson,⁶⁹ M. Wolke,⁷⁵ L. Wollenberg,⁴ C. Wu,⁴⁰ J. F. Wu,^{1,63} L. H. Wu,¹ L. J. Wu,^{1,63} X. Wu,^{12,f} X. H. Wu,³⁵ Y. Wu,⁷¹ Y. J. Wu,³² Z. Wu,^{1,58} L. Xia,^{71,58} X. M. Xian,⁴⁰ T. Xiang,^{47,g} D. Xiao,^{39,j,k} G. Y. Xiao,⁴³ H. Xiao,^{12,f} S. Y. Xiao,¹ Y. L. Xiao,^{12,f} Z. J. Xiao,⁴² C. Xie,⁴³ X. H. Xie,^{47,g} Y. Xie,⁵⁰ Y. G. Xie,^{1,58} Y. H. Xie,⁶ Z. P. Xie,^{71,58} T. Y. Xing,^{1,63} C. F. Xu,^{1,63} C. J. Xu,⁵⁹ G. F. Xu,¹ H. Y. Xu,⁶⁶ Q. J. Xu,¹⁷ Q. N. Xu,³¹ W. Xu,^{1,63} W. L. Xu,⁶⁶ X. P. Xu,⁵⁵ Y. C. Xu,⁷⁸ Z. P. Xu,⁴³ Z. S. Xu,⁶³ F. Yan,^{12,f} L. Yan,^{12,f} W. B. Yan,^{71,58} W. C. Yan,⁸¹ X. Q. Yan,¹ H. J. Yang,^{51,e} H. L. Yang,³⁵ H. X. Yang,¹ Tao Yang,¹ Y. Yang,^{12,f} Y. F. Yang,⁴⁴ Y. X. Yang,^{1,63} Yifan Yang,^{1,63} Z. W. Yang,^{39,j,k} Z. P. Yao,⁵⁰ M. Ye,^{1,58} M. H. Ye,⁸ J. H. Yin,¹ Z. Y. You,⁵⁹ B. X. Yu,^{1,58,63} C. X. Yu,⁴⁴ G. Yu,^{1,63} J. S. Yu,^{26,h} T. Yu,⁷² X. D. Yu,^{47,g} C. Z. Yuan,^{1,63} L. Yuan,² S. C. Yuan,¹ X. Q. Yuan,¹ Y. Yuan,^{1,63} Z. Y. Yuan,⁵⁹ C. X. Yue,⁴⁰ A. A. Zafar,⁷³ F. R. Zeng,⁵⁰ X. Zeng,^{12,f} Y. Zeng,^{26,h} Y. J. Zeng,^{1,63} X. Y. Zhai,³⁵ Y. C. Zhai,⁵⁰ Y. H. Zhan,⁵⁹ A. Q. Zhang,^{1,63} B. L. Zhang,^{1,63} B. X. Zhang,¹ D. H. Zhang,⁴⁴ G. Y. Zhang,²⁰ H. Zhang,⁷¹ H. H. Zhang,⁵⁹ H. H. Zhang,³⁵ H. Q. Zhang,^{1,58,63} H. Y. Zhang,^{1,58} J. J. Zhang,⁵² J. L. Zhang,²¹ J. Q. Zhang,⁴² J. W. Zhang,^{1,58,63} J. X. Zhang,^{39,j,k} J. Y. Zhang,¹ J. Z. Zhang,^{1,63} Jianyu Zhang,⁶³ Jiawei Zhang,^{1,63} L. M. Zhang,⁶¹ L. Q. Zhang,⁵⁹ Lei Zhang,⁴³ P. Zhang,¹ Q. Y. Zhang,^{40,81} Shuihan Zhang,^{1,63} Shulei Zhang,^{26,h} X. D. Zhang,⁴⁶ X. M. Zhang,¹ X. Y. Zhang,⁵⁰ X. Y. Zhang,⁵⁵ Y. Zhang,⁶⁹ Y. Zhang,⁷² Y. T. Zhang,⁸¹ Y. H. Zhang,^{1,58} Yan Zhang,^{71,58} Yao Zhang,¹ Z. H. Zhang,¹ Z. L. Zhang,³⁵ Z. Y. Zhang,⁴⁴ Z. Y. Zhang,⁷⁶ G. Zhao,¹ J. Zhao,⁴⁰ J. Y. Zhao,^{1,63} J. Z. Zhao,^{1,58} Lei Zhao,^{71,58} Ling Zhao,¹ M. G. Zhao,⁴⁴ S. J. Zhao,⁸¹ Y. B. Zhao,^{1,58} Y. X. Zhao,^{32,63} Z. G. Zhao,^{71,58} A. Zhemchugov,^{37,a} B. Zheng,⁷² J. P. Zheng,^{1,58} W. J. Zheng,^{1,63} Y. H. Zheng,⁶³ B. Zhong,⁴² X. Zhong,⁵⁹ H. Zhou,⁵⁰ L. P. Zhou,^{1,63} X. Zhou,⁷⁶ X. K. Zhou,⁶ X. R. Zhou,^{71,58} X. Y. Zhou,⁴⁰ Y. Z. Zhou,^{12,f} J. Zhu,⁴⁴ K. Zhu,¹ K. J. Zhu,^{1,58,63} L. Zhu,³⁵ L. X. Zhu,⁶³ S. H. Zhu,⁷⁰ S. Q. Zhu,⁴³ T. J. Zhu,^{12,f} W. J. Zhu,^{12,f} Y. C. Zhu,^{71,58} Z. A. Zhu,^{1,63} J. H. Zou,¹ and J. Zu^{71,58}

(BESIII Collaboration)

¹*Institute of High Energy Physics, Beijing 100049, People's Republic of China*²*Beihang University, Beijing 100191, People's Republic of China*³*Beijing Institute of Petrochemical Technology, Beijing 102617, People's Republic of China*⁴*Bochum Ruhr-University, D-44780 Bochum, Germany*⁵*Carnegie Mellon University, Pittsburgh, Pennsylvania 15213, USA*⁶*Central China Normal University, Wuhan 430079, People's Republic of China*⁷*Central South University, Changsha 410083, People's Republic of China*⁸*China Center of Advanced Science and Technology, Beijing 100190, People's Republic of China*⁹*China University of Geosciences, Wuhan 430074, People's Republic of China*^{10a}*Chung-Ang University, Seoul 06974, Republic of Korea*¹¹*COMSATS University Islamabad, Lahore Campus, Defence Road, Off Raiwind Road, 54000 Lahore, Pakistan*¹²*Fudan University, Shanghai 200433, People's Republic of China*¹³*G.I. Budker Institute of Nuclear Physics SB RAS (BINP), Novosibirsk 630090, Russia*¹⁴*GSI Helmholtzcentre for Heavy Ion Research GmbH, D-64291 Darmstadt, Germany*¹⁵*Guangxi Normal University, Guilin 541004, People's Republic of China*¹⁶*Guangxi University, Nanning 530004, People's Republic of China*¹⁷*Hangzhou Normal University, Hangzhou 310036, People's Republic of China*¹⁸*Hebei University, Baoding 071002, People's Republic of China*¹⁹*Helmholtz Institute Mainz, Staudinger Weg 18, D-55099 Mainz, Germany*²⁰*Henan Normal University, Xinxiang 453007, People's Republic of China*²¹*Henan University, Kaifeng 475004, People's Republic of China*²²*Henan University of Science and Technology, Luoyang 471003, People's Republic of China*²³*Henan University of Technology, Zhengzhou 450001, People's Republic of China*²⁴*Huangshan College, Huangshan 245000, People's Republic of China*²⁵*Hunan Normal University, Changsha 410081, People's Republic of China*²⁶*Hunan University, Changsha 410082, People's Republic of China*²⁷*Indian Institute of Technology Madras, Chennai 600036, India*²⁸*Indiana University, Bloomington, Indiana 47405, USA*^{29a}*INFN Laboratori Nazionali di Frascati, I-00044 Frascati, Italy*^{29b}*INFN Sezione di Perugia, I-06100 Perugia, Italy*^{29c}*University of Perugia, I-06100 Perugia, Italy*^{30a}*INFN Sezione di Ferrara, I-44122 Ferrara, Italy*^{30b}*University of Ferrara, I-44122 Ferrara, Italy*³¹*Inner Mongolia University, Hohhot 010021, People's Republic of China*

- ³²*Institute of Modern Physics, Lanzhou 730000, People's Republic of China*
- ³³*Institute of Physics and Technology, Peace Avenue 54B, Ulaanbaatar 13330, Mongolia*
- ³⁴*Instituto de Alta Investigación, Universidad de Tarapacá, Casilla 7D, Arica, Chile*
- ³⁵*Jilin University, Changchun 130012, People's Republic of China*
- ³⁶*Johannes Gutenberg University of Mainz, Johann-Joachim-Becher-Weg 45, D-55099 Mainz, Germany*
- ³⁷*Joint Institute for Nuclear Research, 141980 Dubna, Moscow region, Russia*
- ³⁸*Justus-Liebig-Universität Giessen, II. Physikalisches Institut, Heinrich-Buff-Ring 16, D-35392 Giessen, Germany*
- ³⁹*Lanzhou University, Lanzhou 730000, People's Republic of China*
- ⁴⁰*Liaoning Normal University, Dalian 116029, People's Republic of China*
- ⁴¹*Liaoning University, Shenyang 110036, People's Republic of China*
- ⁴²*Nanjing Normal University, Nanjing 210023, People's Republic of China*
- ⁴³*Nanjing University, Nanjing 210093, People's Republic of China*
- ⁴⁴*Nankai University, Tianjin 300071, People's Republic of China*
- ⁴⁵*National Centre for Nuclear Research, Warsaw 02-093, Poland*
- ⁴⁶*North China Electric Power University, Beijing 102206, People's Republic of China*
- ⁴⁷*Peking University, Beijing 100871, People's Republic of China*
- ⁴⁸*Qufu Normal University, Qufu 273165, People's Republic of China*
- ⁴⁹*Shandong Normal University, Jinan 250014, People's Republic of China*
- ⁵⁰*Shandong University, Jinan 250100, People's Republic of China*
- ⁵¹*Shanghai Jiao Tong University, Shanghai 200240, People's Republic of China*
- ⁵²*Shanxi Normal University, Linfen 041004, People's Republic of China*
- ⁵³*Shanxi University, Taiyuan 030006, People's Republic of China*
- ⁵⁴*Sichuan University, Chengdu 610064, People's Republic of China*
- ⁵⁵*Soochow University, Suzhou 215006, People's Republic of China*
- ⁵⁶*South China Normal University, Guangzhou 510006, People's Republic of China*
- ⁵⁷*Southeast University, Nanjing 211100, People's Republic of China*
- ⁵⁸*State Key Laboratory of Particle Detection and Electronics, Beijing 100049, Hefei 230026, People's Republic of China*
- ⁵⁹*Sun Yat-Sen University, Guangzhou 510275, People's Republic of China*
- ⁶⁰*Suranaree University of Technology, University Avenue 111, Nakhon Ratchasima 30000, Thailand*
- ⁶¹*Tsinghua University, Beijing 100084, People's Republic of China*
- ^{62a}*Turkish Accelerator Center Particle Factory Group, Istinye University, 34010 Istanbul, Turkey*
- ^{62b}*Near East University, Nicosia, North Cyprus 99138, Mersin 10, Turkey*
- ⁶³*University of Chinese Academy of Sciences, Beijing 100049, People's Republic of China*
- ⁶⁴*University of Groningen, NL-9747 AA Groningen, The Netherlands*
- ⁶⁵*University of Hawaii, Honolulu, Hawaii 96822, USA*
- ⁶⁶*University of Jinan, Jinan 250022, People's Republic of China*
- ⁶⁷*University of Manchester, Oxford Road, Manchester M13 9PL, United Kingdom*
- ⁶⁸*University of Muenster, Wilhelm-Klemm-Strasse 9, 48149 Muenster, Germany*
- ⁶⁹*University of Oxford, Keble Road, Oxford OX13RH, United Kingdom*
- ⁷⁰*University of Science and Technology Liaoning, Anshan 114051, People's Republic of China*
- ⁷¹*University of Science and Technology of China, Hefei 230026, People's Republic of China*
- ⁷²*University of South China, Hengyang 421001, People's Republic of China*
- ⁷³*University of the Punjab, Lahore-54590, Pakistan*
- ^{74a}*University of Turin and INFN, University of Turin, I-10125 Turin, Italy*
- ^{74b}*University of Eastern Piedmont, I-15121 Alessandria, Italy*
- ^{74c}*INFN, I-10125 Turin, Italy*
- ⁷⁵*Uppsala University, Box 516, SE-75120 Uppsala, Sweden*
- ⁷⁶*Wuhan University, Wuhan 430072, People's Republic of China*
- ⁷⁷*Xinyang Normal University, Xinyang 464000, People's Republic of China*
- ⁷⁸*Yantai University, Yantai 264005, People's Republic of China*
- ⁷⁹*Yunnan University, Kunming 650500, People's Republic of China*
- ⁸⁰*Zhejiang University, Hangzhou 310027, People's Republic of China*
- ⁸¹*Zhengzhou University, Zhengzhou 450001, People's Republic of China*

^aAlso at the Moscow Institute of Physics and Technology, Moscow 141700, Russia.

^bAlso at the Novosibirsk State University, Novosibirsk 630090, Russia.

^cAlso at the NRC "Kurchatov Institute", PNPI, 188300 Gatchina, Russia.

^dAlso at Goethe University Frankfurt, 60323 Frankfurt am Main, Germany.

 (Received 26 July 2023; accepted 31 October 2023; published 4 December 2023)

Using e^+e^- collision data with an integrated luminosity of 7.33 fb^{-1} collected at center-of-mass energies between 4.128 and 4.226 GeV with the BESIII detector operating at the BEPCII collider, the branching fraction of the leptonic decay $D_s^+ \rightarrow \mu^+\nu_\mu$ is measured to be $(0.5294 \pm 0.0108_{\text{stat}} \pm 0.0085_{\text{syst}})\%$. Based on this, the product of the D_s^+ decay constant $f_{D_s^+}$ and the magnitude of the $c \rightarrow s$ quark mixing matrix element $|V_{cs}|$ is determined to be $f_{D_s^+}|V_{cs}| = 241.8 \pm 2.5_{\text{stat}} \pm 2.2_{\text{syst}} \text{ MeV}$. Using the value of $|V_{cs}|$ given by the global standard model fit, $f_{D_s^+}$ is found to be $248.4 \pm 2.5_{\text{stat}} \pm 2.2_{\text{syst}} \text{ MeV}$. Alternatively, using the value of $f_{D_s^+}$ from a recent lattice quantum chromodynamics calculation, $|V_{cs}|$ is determined to be $0.968 \pm 0.010_{\text{stat}} \pm 0.009_{\text{syst}}$.

DOI: [10.1103/PhysRevD.108.112001](https://doi.org/10.1103/PhysRevD.108.112001)

I. INTRODUCTION

Experimental studies of the leptonic decay $D_s^+ \rightarrow \ell^+\nu_\ell$ ($\ell = e, \mu$ or τ) are important to explore both the strong and weak interactions in the charm quark sector. In the standard model (SM), the $D_s^+ \rightarrow \ell^+\nu_\ell$ decay partial width is given by [1]

$$\Gamma_{D_s^+ \rightarrow \ell^+\nu_\ell} = \frac{G_F^2}{8\pi} |V_{cs}|^2 f_{D_s^+}^2 m_\ell^2 m_{D_s^+} \left(1 - \frac{m_\ell^2}{m_{D_s^+}^2}\right)^2, \quad (1)$$

where G_F is the Fermi coupling constant, m_ℓ is the lepton mass, $m_{D_s^+}$ is the D_s^+ mass, $f_{D_s^+}$ is the D_s^+ decay constant, and $|V_{cs}|$ is the magnitude of the $c \rightarrow s$ Cabibbo-Kobayashi-Maskawa (CKM) matrix element.

In recent years, many studies of $D_s^+ \rightarrow \ell^+\nu_\ell$ have been performed by the CLEO [2–4], BABAR [5], Belle [6], and

BESIII [7–13] experiments. The experimental precision of $f_{D_s^+}$, however, is still worse than the lattice quantum chromodynamics (LQCD) calculation [14,15]. Intensive experimental studies of $D_s^+ \rightarrow \ell^+\nu_\ell$ can determine $f_{D_s^+}$ and $|V_{cs}|$ with improved precision and can thereby calibrate various theoretical calculations of $f_{D_s^+}$ [14,16–25] and test the unitarity of the CKM matrix.

In addition, scrutinizing lepton flavor universality (LFU) violation in $D_s^+ \rightarrow \ell^+\nu_\ell$ decays offers an important test of the SM [26–34]. In the SM, the ratio of the branching fraction (BF) of $D_s^+ \rightarrow \tau^+\nu_\tau$ over that of $D_s^+ \rightarrow \mu^+\nu_\mu$ is predicted to be 9.75 with a negligible uncertainty, and hence any observed deviation from this value would mean a sign of new physics beyond the SM. Some hints of LFU violation in semileptonic B decays were reported by BABAR, LHCb, and Belle [26–33]. The measured BF ratios $\mathcal{R}_{D^{(*)} \rightarrow \ell^+ \nu_\ell}^{\tau/\ell} = \mathcal{B}_{B \rightarrow \bar{D}^{(*)} \tau^+ \nu_\tau} / \mathcal{B}_{B \rightarrow \bar{D}^{(*)} \ell^+ \nu_\ell}$ deviate from the SM predictions by about 3.3σ [34]. A test of LFU with $D_s^+ \rightarrow \ell^+\nu_\ell$ decays may shed light on this tension.

In this paper, we report an improved measurement of the BF of the $D_s^+ \rightarrow \mu^+\nu_\mu$ decay by analyzing 7.33 fb^{-1} of e^+e^- collision data collected with the BESIII detector at center-of-mass energies of $E_{\text{cm}} = 4.128, 4.156, 4.178, 4.189, 4.199, 4.209, 4.219, \text{ and } 4.226 \text{ GeV}$. Charge-conjugate (*c.c.*) modes are always implied in the text. Benefiting from a larger data sample, more tag modes, and measurement from muon identifier modules, the results obtained in this work supersede the previous BESIII measurement with the muon identifier modules using data at $E_{\text{cm}} = 4.178 \text{ GeV}$ [8] and the measurement without the muon identifier modules using data at E_{cm} between 4.178 and 4.226 GeV [9].

II. BESIII DETECTOR AND MONTE CARLO SIMULATION

The BESIII detector is a magnetic spectrometer [35] located at the Beijing Electron Positron Collider (BEPCII) [36]. The cylindrical core of the BESIII detector consists of a helium-based multilayer drift chamber (MDC), a plastic

^eAlso at Key Laboratory for Particle Physics, Astrophysics and Cosmology, Ministry of Education; Shanghai Key Laboratory for Particle Physics and Cosmology; Institute of Nuclear and Particle Physics, Shanghai 200240, People's Republic of China.

^fAlso at Key Laboratory of Nuclear Physics and Ion-beam Application (MOE) and Institute of Modern Physics, Fudan University, Shanghai 200443, People's Republic of China.

^gAlso at State Key Laboratory of Nuclear Physics and Technology, Peking University, Beijing 100871, People's Republic of China.

^hAlso at School of Physics and Electronics, Hunan University, Changsha 410082, China.

ⁱAlso at Guangdong Provincial Key Laboratory of Nuclear Science, Institute of Quantum Matter, South China Normal University, Guangzhou 510006, China.

^jAlso at Frontiers Science Center for Rare Isotopes, Lanzhou University, Lanzhou 730000, People's Republic of China.

^kAlso at Lanzhou Center for Theoretical Physics, Lanzhou University, Lanzhou 730000, People's Republic of China.

^lAlso at the Department of Mathematical Sciences, IBA, Karachi 75270, Pakistan.

Published by the American Physical Society under the terms of the Creative Commons Attribution 4.0 International license. Further distribution of this work must maintain attribution to the author(s) and the published article's title, journal citation, and DOI. Funded by SCOAP³.

TABLE I. The integrated luminosities and requirements on M_{BC} for the ST candidates at various energy points.

E_{cm} (GeV)	Luminosity (pb^{-1})	M_{BC} (GeV/ c^2)
4.128	401.5	(2.010, 2.061)
4.157	408.7	(2.010, 2.070)
4.178	3189.0	(2.010, 2.073)
4.189	569.8	(2.010, 2.076)
4.199	526.0	(2.010, 2.079)
4.209	571.7	(2.010, 2.082)
4.219	568.7	(2.010, 2.085)
4.226	1091.7	(2.010, 2.088)

scintillator time-of-flight system (TOF), and a CsI (TI) electromagnetic calorimeter (EMC), which are all enclosed in a superconducting solenoidal magnet providing a 1.0 T magnetic field. The solenoid is supported by an octagonal flux-return yoke with resistive plate counter muon identifier modules interleaved with steel. The solid angle coverage for detecting charged particles is 93% over 4π . The charged-particle momentum resolution at 1 GeV/ c is 0.5%, and the resolution of the specific ionization energy loss (dE/dx) is 6% for the electrons from Bhabha scattering. The EMC measures photon energies with a resolution of 2.5% (5%) at 1 GeV in the barrel (end cap) region. The time resolution of the TOF barrel part is 68 ps, while that of the end cap part is 110 ps. The end cap TOF system was upgraded in 2015 using multigap resistive plate chamber technology, providing a time resolution of 60 ps [37,38]. Approximately 83% of the data used here was collected after this upgrade, and the corresponding luminosities [39,40] at each energy are given in Table I. More details about the design and performance of the BESIII detector are given in Ref. [35].

Simulated samples produced with GEANT4-based [41] Monte Carlo (MC) software, which includes the geometric description of the BESIII detector and the detector response, are used to determine the detection efficiency and to estimate background contributions. The simulations include the beam energy spread and initial state radiation in the e^+e^- annihilations modeled with the generator KKMC [42,43]. An inclusive MC sample with an equivalent luminosity of 40 times that of the data is produced at center-of-mass energies between 4.128 and 4.226 GeV. It includes open-charm processes, initial state radiation (ISR) production of $\psi(3770)$, ISR production of $\psi(3686)$, ISR production of J/ψ , $q\bar{q}$ ($q = u, d, s$) continuum processes, along with Bhabha scattering, $\mu^+\mu^-$, $\tau^+\tau^-$, and $\gamma\gamma$ events. In the simulation, the production of open-charm processes directly produced via e^+e^- annihilations is modeled with the generator CONEXC [44], and their subsequent decays are modeled by EVTGen [45,46] with known BFs from the Particle Data Group (PDG) [47]. The input cross section of $e^+e^- \rightarrow D_s^\pm D_s^{*\mp}$ is based on the cross section measurement in the energy range from threshold to 4.7 GeV. The ISR production of vector charmonium(like) states and the

continuum processes are incorporated in KKMC [42,43]. The remaining unknown decays of the charmonium states are modeled by Lundcharm [48,49]. Final state radiation is incorporated using PHOTOS [50].

III. METHOD

At E_{cm} from 4.128 to 4.226 GeV, the D_s^\pm mesons are produced mainly through the process $e^+e^- \rightarrow D_s^{*\pm} D_s^\mp \rightarrow \gamma(\pi^0) D_s^\pm D_s^\mp$. A single-tag (ST) sample is selected by fully reconstructing a D_s^- meson in one of several ‘‘tag’’ modes. Those in which the ST D_s^- , the transition $\gamma(\pi^0)$ of the D_s^{*+} decay, and the signal D_s^+ decay of interest are simultaneously reconstructed are called the double-tag (DT) sample. Then, the BF of $D_s^+ \rightarrow \mu^+\nu_\mu$ is determined by

$$\mathcal{B}_{D_s^+ \rightarrow \mu^+\nu_\mu} = \frac{N_{\text{DT}}}{N_{\text{ST}} \cdot \epsilon_{\gamma(\pi^0)\mu^+\nu_\mu}}, \quad (2)$$

where N_{DT} is the DT yield in data; $N_{\text{ST}} = \sum_i N_{\text{ST}}^i$ is the total ST yield in data summing over tag mode i ; $\epsilon_{\gamma(\pi^0)\mu^+\nu_\mu} = \sum_i (N_{\text{ST}}^i / N_{\text{ST}}) \cdot (\epsilon_{\text{DT}}^i / \epsilon_{\text{ST}}^i)$ is the effective signal efficiency of detecting $D_s^+ \rightarrow \mu^+\nu_\mu$ in the presence of the ST D_s^- candidate, averaged by the ST yields in data; and ϵ_{DT}^i and ϵ_{ST}^i are the detection efficiencies of the DT and ST candidates, respectively.

IV. SINGLE-TAG SELECTION

The ST D_s^- mesons are reconstructed using 16 hadronic D_s^- decay modes: $K^+K^-\pi^-$, $K^+K^-\pi^-\pi^0$, $\pi^+\pi^-\pi^-$, $K_S^0K^-$, $K_S^0K^-\pi^0$, $K^-\pi^+\pi^-$, $K_S^0K_S^0\pi^-$, $K_S^0K^+\pi^-\pi^-$, $K_S^0K^-\pi^+\pi^-$, $\eta_{\gamma\gamma}\pi^-$, $\eta_{\pi^+\pi^-\pi^0}\pi^-$, $\eta'_{\pi^+\pi^-\eta_{\gamma\gamma}}\pi^-$, $\eta'_{\gamma\rho}\pi^-$, $\eta_{\gamma\gamma}\rho^-$, $\eta_{\pi^+\pi^-\pi^0}\rho^-$, and $\eta_{\gamma\gamma}\pi^+\pi^-\pi^-$, where the subscripts on the $\eta(\eta')$ represent the decay modes used to reconstruct the $\eta(\eta')$.

All charged tracks except for those from K_S^0 decays must originate from the interaction point (IP) with a distance of closest approach less than 1 cm in the transverse plane and less than 10 cm along the z axis. The polar angle (θ) is required to be within the MDC acceptance $|\cos\theta| < 0.93$, where θ is defined with respect to the symmetry axis of the MDC taken as the z axis. Measurements of the dE/dx in the MDC and the flight time in the TOF are combined for particle identification (PID) by calculating confidence levels for the pion and kaon hypotheses (CL_π , CL_K). Kaon (pion) candidates are required to satisfy $CL_{K(\pi)} > CL_{\pi(K)}$.

To select K_S^0 candidates, pairs of oppositely charged tracks with distance of closest approach to the IP less than 20 cm along the z axis are assigned as $\pi^+\pi^-$ without PID requirements. These $\pi^+\pi^-$ combinations are required to have an invariant mass within ± 12 MeV of the nominal K_S^0 mass [47] and a decay length greater than twice the vertex resolution away from the IP.

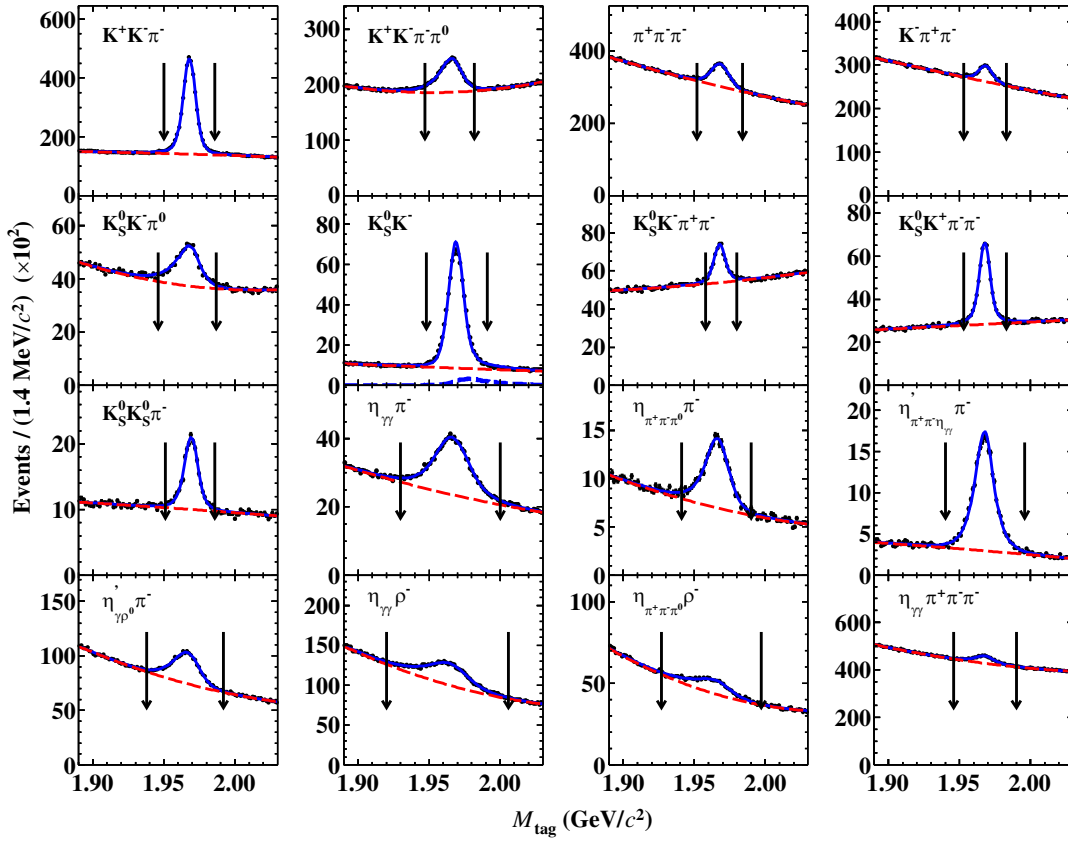


FIG. 1. Fits to the M_{tag} distributions of ST D_s^- candidates selected from data at all energy points, where the points with error bars are data, the solid curve shows the best fit, and the red dashed line shows the shape of the combinatorial backgrounds. In the fit to the M_{tag} distribution for $D_s^- \rightarrow K_S^0 K^-$, the blue dashed curve shows the shape of $D^- \rightarrow K_S^0 \pi^-$.

The π^0 and η mesons are reconstructed via their decays to $\gamma\gamma$. Here, the γ candidates are identified using isolated showers in the EMC. The deposited energy of each shower must be greater than 25 (50) MeV in the EMC barrel (end cap) region [35]. To suppress electronic noise and showers unrelated to the event, the difference between the EMC time and the event start time is required to be within [0, 700] ns [35]. The opening angle between a shower and the nearest charged track has to be greater than 10° . The $\gamma\gamma$ combinations with invariant masses $M_{\gamma\gamma} \in (0.115, 0.150)$ and $(0.500, 0.570)$ GeV/c^2 are regarded as π^0 and η candidates, respectively. A kinematic fit is further performed to constrain $M_{\gamma\gamma}$ to the π^0 or η nominal mass [47].

The η candidates for the $\eta\pi^-$ ST channel are also reconstructed via $\pi^0\pi^+\pi^-$ final states with an invariant mass within $(0.53, 0.57)$ GeV/c^2 . The η' mesons are reconstructed via two decay modes, $\eta\pi^+\pi^-$ and $\gamma\rho^0$, whose invariant masses are required to be within $(0.946, 0.970)$ and $(0.940, 0.976)$ GeV/c^2 , respectively. In addition, the minimum energy of the γ from $\eta' \rightarrow \gamma\rho^0$ decays must be greater than 0.1 GeV. The ρ^0 and ρ^+ mesons are reconstructed from $\pi^+\pi^-$ and $\pi^+\pi^0$ combinations whose invariant masses are required to be within $(0.67, 0.87)$ GeV/c^2 .

The momentum of any pion not originating from a K_S^0 , η , or η' decay is required to be greater than 0.1 GeV/c to reject transition pions from D^* decays. When selecting $\pi^+\pi^-\pi^-$ and $K^-\pi^+\pi^-$ combinations, peaking backgrounds from $K_S^0\pi^-$ and $K_S^0K^-$ components are rejected by requiring that the invariant mass of any $\pi^+\pi^-$ combination satisfy $|M_{\pi^+\pi^-} - M_{K_S^0}| > 0.030$ GeV/c^2 [47].

The beam-constrained mass of the ST D_s^- candidate

$$M_{\text{BC}} \equiv \sqrt{(E_{\text{cm}}/2)^2/c^4 - |\vec{p}_{D_s^-}|^2/c^2} \quad (3)$$

is used to suppress the non- $D_s^+D_s^{*-}$ events, where $\vec{p}_{D_s^-}$ is the momentum of the ST D_s^- candidate. The M_{BC} of the direct D_s^- candidate form a peak around 2.04 GeV/c^2 with a resolution of (1.9–2.8) MeV, while it ranges in $(2.01, 2.07)$ GeV/c^2 for the indirect D_s^- candidate. The requirements on M_{BC} for the eight center-of-mass energies are listed in Table I and retain the D_s^- mesons from both the e^+e^- annihilation and the D_s^{*-} decay. The efficiency loss due to the M_{BC} selection is not more than 3% for each energy point. In each event, we only keep the candidate with the D_s^- recoil mass

TABLE II. The M_{tag} requirements, ST yields in data (N_{ST}^i), ST efficiencies (ϵ_{ST}^i), and effective signal efficiencies with transition $\gamma(\pi^0)$ matched ($\epsilon_{\gamma(\pi^0)\mu^+\nu_\mu}^{i,\text{matched}}$) of various tag modes obtained from data at $E_{\text{cm}} = 4.178$ GeV. The uncertainties are statistical only. The $\epsilon_{\gamma(\pi^0)\mu^+\nu_\mu}^{i,\text{matched}}$ varies within 37% for different tag modes, which are mainly caused by the significantly different signal environments for some tag modes containing low momentum photon and pions in the signal and inclusive MC samples. The ST efficiency of $D_s^- \rightarrow K_S^0 K^- \pi^+ \pi^-$ is $\sim 12\%$ lower than that of $D_s^- \rightarrow K_S^0 K^- \pi^+ \pi^-$, due to more low momentum charged particles from different subresonances.

Tag mode	M_{tag} (GeV/ c^2)	N_{ST}^i	ϵ_{ST}^i (%)	$\epsilon_{\gamma(\pi^0)\mu^+\nu_\mu}^{i,\text{matched}}$ (%)
$K^+ K^- \pi^-$	(1.950, 1.986)	13717 \pm 608	40.92 \pm 0.02	49.25 \pm 0.21
$K^+ K^- \pi^- \pi^0$	(1.947, 1.982)	42119 \pm 851	11.77 \pm 0.01	58.33 \pm 0.74
$\pi^- \pi^+ \pi^-$	(1.952, 1.984)	36497 \pm 873	52.13 \pm 0.05	51.16 \pm 0.19
$K_S^0 K^-$	(1.948, 1.991)	30956 \pm 261	47.63 \pm 0.05	50.32 \pm 0.23
$K_S^0 K^- \pi^0$	(1.946, 1.987)	11182 \pm 449	17.01 \pm 0.04	58.42 \pm 0.74
$K^- \pi^+ \pi^-$	(1.953, 1.983)	16514 \pm 632	45.42 \pm 0.07	51.44 \pm 0.41
$K_S^0 K_S^0 \pi^-$	(1.951, 1.986)	5088 \pm 149	22.82 \pm 0.07	51.97 \pm 0.91
$K_S^0 K^+ \pi^- \pi^-$	(1.953, 1.983)	14855 \pm 235	21.12 \pm 0.04	50.72 \pm 0.79
$K_S^0 K^- \pi^+ \pi^-$	(1.958, 1.980)	7621 \pm 270	18.51 \pm 0.05	52.15 \pm 0.43
$\eta \pi^-$	(1.930, 2.000)	19239 \pm 468	48.79 \pm 0.06	54.12 \pm 0.20
$\eta_{\pi^+ \pi^- \pi^0} \pi^-$	(1.941, 1.990)	5693 \pm 201	23.49 \pm 0.07	55.51 \pm 0.34
$\eta'_{\eta \pi^+ \pi^-} \pi^-$	(1.940, 1.996)	9730 \pm 140	25.26 \pm 0.05	55.12 \pm 0.31
$\eta'_{\gamma \rho} \pi^-$	(1.938, 1.992)	24698 \pm 656	32.53 \pm 0.04	54.10 \pm 0.26
$\eta \rho^-$	(1.920, 2.006)	39670 \pm 1673	19.88 \pm 0.02	66.92 \pm 0.37
$\eta_{\pi^+ \pi^- \pi^0} \rho^-$	(1.927, 1.997)	10504 \pm 928	9.23 \pm 0.02	67.48 \pm 0.57
$\eta_{\gamma \gamma} \pi^+ \pi^- \pi^-$	(1.946, 1.990)	23417 \pm 1232	24.84 \pm 0.04	63.74 \pm 0.32

$$M_{\text{rec}} \equiv \sqrt{(E_{\text{cm}} - \sqrt{|\vec{p}_{D_s^-}|^2 c^2 + m_{D_s^-}^2 c^4})^2 / c^4 - |\vec{p}_{D_s^-}|^2 / c^2} \quad (4)$$

closest to the nominal D_s^{*+} mass [47] per tag mode per charge. The probability of the best candidate selection for individual tag modes ranges in (82–99)%. Figure 1 shows the invariant mass (M_{tag}) spectra of the accepted ST candidates with all datasets.

At each energy point, the ST yield for each tag mode is obtained by a fit to the corresponding M_{tag} spectrum. The signal is described by the MC-simulated shape convolved with a Gaussian function representing the resolution difference between data and MC simulation. For the tag mode $D_s^- \rightarrow K_S^0 K^-$, the peaking background from $D^- \rightarrow K_S^0 \pi^-$ is described by the MC-simulated shape smeared with the same Gaussian function as used in the signal shape with the magnitude free in the fit. The nonpeaking background is modeled by a second- or third-order Chebychev polynomial function, which is validated with the inclusive MC sample. The fit results of M_{tag} summed over all energy points are shown in Fig. 1. The events in the signal regions are kept for further analysis. The fraction of the $e^+ e^- \rightarrow \gamma(\pi^0) D_s^\pm D_s^\mp$ process is about (0.7–1.1)% in the fitted yield of ST D_s^- mesons for each tag mode and has been subtracted away from individual fitted ST yield. As an example, the ST yields in data and the ST efficiencies at 4.178 GeV are shown in

Table II. The total ST yields at the different energy points are summarized in Table III.

V. DOUBLE-TAG SELECTION

We select candidates for the transition $\gamma(\pi^0)$ from the D_s^{*+} decay among the unused particles recoiling against the ST D_s^- , by using the kinematic variable

TABLE III. The ST yields in data (N_{ST}), the weighted signal efficiencies with transition $\gamma(\pi^0)$ matched ($\epsilon_{\gamma(\pi^0)\mu^+\nu_\mu}^{\text{matched}}$), and signal efficiencies unmatched within 20° ($\epsilon_{\gamma(\pi^0)\mu^+\nu_\mu}^{\text{unmatched}}$) for various energy points. The uncertainties are unmatched statistical only. The weighted signal efficiencies monotonically decrease with center-of-mass energy, mainly due to different ISR and final state effects as well as correction factors for muon identification.

E_{cm} (GeV)	N_{ST}	$\epsilon_{\gamma(\pi^0)\mu^+\nu_\mu}^{\text{matched}}$ (%)	$\epsilon_{\gamma(\pi^0)\mu^+\nu_\mu}^{\text{unmatched}}$ (%)
4.128	38203 \pm 1794	57.48 \pm 0.14	5.91 \pm 0.05
4.157	55280 \pm 971	56.26 \pm 0.13	5.96 \pm 0.05
4.178	435100 \pm 2926	54.35 \pm 0.12	5.64 \pm 0.05
4.189	72852 \pm 1030	52.76 \pm 0.12	5.67 \pm 0.05
4.199	68054 \pm 1136	53.31 \pm 0.12	5.94 \pm 0.05
4.209	68608 \pm 1281	51.12 \pm 0.12	5.70 \pm 0.05
4.219	58151 \pm 1159	49.47 \pm 0.12	5.41 \pm 0.04
4.226	91218 \pm 1739	49.66 \pm 0.12	5.62 \pm 0.05

$$\Delta E \equiv E_{\text{cm}} - E_{\text{tag}} - \sqrt{|\vec{p}_{\text{tag}} - \vec{p}_{\gamma(\pi^0)}|^2/c^4 + m_{D_s^+}^2} - E_{\gamma(\pi^0)}, \quad (5)$$

where E_i and \vec{p}_i , with $i = [\gamma(\pi^0) \text{ or tag}]$, denote the energy and momentum of particle i . We loop over all remaining γ or π^0 candidates and choose the one giving a minimum $|\Delta E|$. The events with $\Delta E \in (-0.05, 0.10)$ GeV are accepted.

In the presence of ST D_s^- and transition $\gamma(\pi^0)$, the $D_s^+ \rightarrow \mu^+ \nu_\mu$ candidates are selected using the remaining neutral and charged tracks. The muon candidate is required to have an opposite charge to the ST D_s^- meson and deposited energy in the EMC within (0.0, 0.3) GeV. To separate muons from hadrons, fulfill requirements on the muon hit depth (d_{μ^+}) in the muon counter with dependence of p_{μ^+} and flight direction $\cos\theta$ in the muon identifier modules. To consider the p_{μ^+} and d_{μ^+} dependence, we examine the distributions of d_{μ^+} versus p_{μ^+} using $e^+e^- \rightarrow (\gamma)\mu^+\mu^-$ candidates selected from data, as shown in Fig. 2. The $|\cos\theta_{\mu^+}|$ and p_{μ^+} dependent requirements on d_{μ^+} are shown in Table IV.

To suppress backgrounds with extra photon(s), the maximum energy of the unused showers in the DT selection ($E_{\text{max}}^{\text{extray}}$) is required to be less than 0.3 GeV. No any additional charged track is in the event. The yield of signal events is determined by a fit to the distribution of the kinematic variable

$$M_{\text{miss}}^2 \equiv E_\nu^2/c^4 - |\vec{p}_\nu|^2/c^2. \quad (6)$$

Here, $E_\nu \equiv E_{\text{cm}} - E_{\text{tag}} - E_{\gamma(\pi^0)} - E_\mu$ and $\vec{p}_\nu \equiv -\vec{p}_{\text{tag}} - \vec{p}_{\gamma(\pi^0)} - \vec{p}_\mu$, where E_μ and \vec{p}_μ denote the energy and momentum of the muon, respectively. M_{miss}^2 is the missing mass square of the undetected neutrino. To improve the M_{miss}^2 resolution, the candidate tracks plus the missing neutrino are subjected to a four-constraint kinematic fit requiring energy and momentum conservation. In addition, the invariant masses of the two D_s mesons are constrained

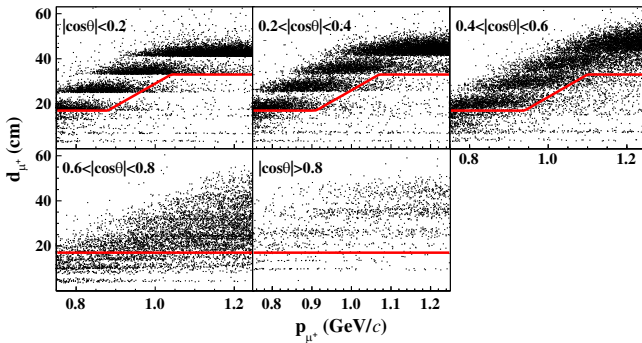


FIG. 2. The d_{μ^+} vs p_{μ^+} of muon candidates of the $e^+e^- \rightarrow \gamma\mu^+\mu^-$ processes in different $|\cos\theta|$ regions from data.

TABLE IV. The $\cos\theta_{\mu^+}$ and p_{μ^+} dependent requirements of d_{μ^+} for muon candidates. To compute the d_{μ^+} requirements, the momentum p_{μ^+} is taken in units of GeV/ c .

$ \cos\theta_{\mu^+} $	p_{μ^+} (GeV/ c)	d_{μ^+} (cm)
(0.00, 0.20)	$p_{\mu^+} \leq 0.88$	> 17.0
	$0.88 < p_{\mu^+} < 1.04$	$> 100.0 \times p_{\mu^+} - 71.0$
	$p_{\mu^+} \geq 1.04$	> 33.0
(0.20, 0.40)	$p_{\mu^+} \leq 0.91$	> 17.0
	$0.91 < p_{\mu^+} < 1.07$	$> 100.0 \times p_{\mu^+} - 74.0$
	$p_{\mu^+} \geq 1.07$	> 33.0
(0.40, 0.60)	$p_{\mu^+} \leq 0.94$	> 17.0
	$0.94 < p_{\mu^+} < 1.10$	$> 100.0 \times p_{\mu^+} - 77.0$
	$p_{\mu^+} \geq 1.10$	> 33.0
(0.60, 0.80)		> 17.0
(0.80, 0.93)		> 17.0

to the known D_s mass, and the invariant mass of the $D_s^- \gamma(\pi^0)$ or $D_s^+ \gamma(\pi^0)$ combination is constrained to the nominal D_s^* mass. The combination with the minimum χ^2 is kept. Figure 3 shows the M_{miss}^2 distribution for the accepted DT candidate events in data.

The efficiencies of the DT reconstruction are determined with the signal MC samples. Dividing them by the ST efficiencies determined with the inclusive MC sample

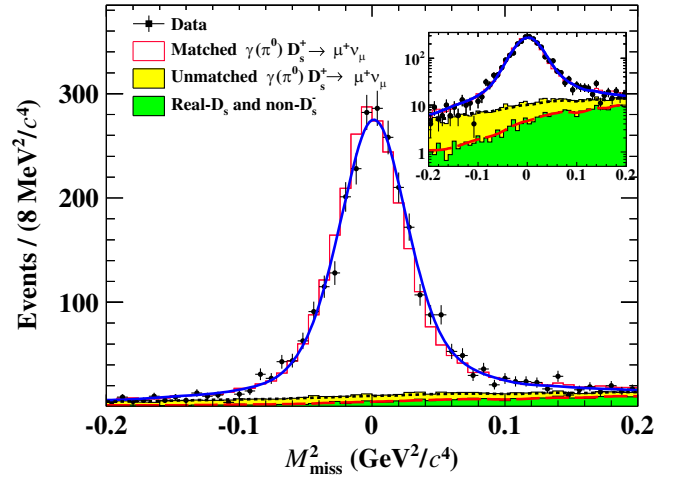


FIG. 3. Fit to the M_{miss}^2 distribution of the accepted candidates for $D_s^+ \rightarrow \mu^+ \nu_\mu$ in data. The inset plot shows the same distribution in a log scale. The points with error bars are data, the blue solid curve shows the best fit, and the red dashed curve shows the fitted combinatorial background shape. Events between the red dashed and black dotted curves (yellow filled histogram) are from signals with transition $\gamma(\pi^0)$ unmatched. Events between the black dashed and the pink histogram are from signals with the transition $\gamma(\pi^0)$ matched. The green filled histogram is the combined real- D_s^- and non- D_s^- background derived from the inclusive MC sample after normalization.

yields the corresponding efficiencies of the $\gamma(\pi^0)\mu^+\nu_\mu$ reconstruction. The efficiency averaged over all tag modes is then determined from

$$\epsilon_{\gamma(\pi^0)\mu^+\nu_\mu} = f_{\mu\text{PID}}^{\text{cor}} f_{\text{tag bias}}^{\text{cor}} \sum_i (N_{\text{ST}}^i \epsilon_{\text{DT}}^i) / (N_{\text{ST}}^{\text{tot}} \epsilon_{\text{ST}}^i). \quad (7)$$

In the above equation, the correction factor $f_{\mu\text{PID}}^{\text{cor}}$ accounts for the differences of μ^+ identification efficiencies between data and MC simulation. It is non-negligible mainly due to the imperfect simulation of d_{μ^+} [8]. The energy point dependent correction factors for μ^+ identification efficiencies are (87.6–93.9)% with uncertainties of (0.4–1.1)%, depending on the data taking status. These efficiencies are estimated using $e^+e^- \rightarrow \gamma\mu^+\mu^-$ samples and reweighted by the μ^+ two-dimensional distribution in $|\cos\theta_{\mu^+}|$ and p_{μ^+} of $D_s^+ \rightarrow \mu^+\nu_\mu$.

The correction factor $f_{\text{tag bias}}^{\text{cor}}$ takes into account the differences of the ST efficiencies in the inclusive and signal MC samples due to different track multiplicities. This may cause incomplete cancellation of the uncertainties of the ST efficiencies. It is estimated to be about 99.57% after considering the differences of the efficiencies of tracking or PID of K^\pm and π^\pm , as well as the selections of neutral particles between data and MC simulation.

In this analysis, the shapes of signal candidates are divided into two types: one describes the signal candidates with transition $\gamma(\pi^0)$ matched, and another describes the signal candidates unmatched. The matched type requires the angle between the flight direction of the reconstructed $\gamma(\pi^0)$ and that of MC truth to be less than 20° in an event; otherwise, the event is classified as the unmatched type. Both event types have real $D_s^+ \rightarrow \mu^+\nu_\mu$, but the matched type forms the peak, and the unmatched type forms the combinatorial shape in the M_{miss}^2 distribution. The fraction of the unmatched $\gamma(\pi^0)D_s^+ \rightarrow \mu^+\nu_\mu$ is within (9–10)% for each energy point. The average signal efficiencies for finding $\gamma(\pi^0)\mu^+\nu_\mu$ at various energy points are shown in Table III.

The background includes two components. One is the events with wrongly tagged D_s^- decays (“non- D_s^- background”), and another is with correctly tagged D_s^- decays but incorporating particle misidentifications (“real- D_s^- background”) which is mainly from $D_s^+ \rightarrow \tau^+(\rightarrow \pi^+\bar{\nu}_\tau)\nu_\tau$ decay. Studies on the inclusive MC sample show that the two components make comparable contributions and do not peak in the signal region. The total background fraction is about 8.2%.

VI. BRANCHING FRACTION MEASUREMENT

To obtain the BF of $D_s^+ \rightarrow \mu^+\nu_\mu$, we perform a simultaneous fit to the M_{miss}^2 distributions at the eight energy points. The BF of $D_s^+ \rightarrow \mu^+\nu_\mu$ at different energy points is the common parameter in the fit. The signal shapes with

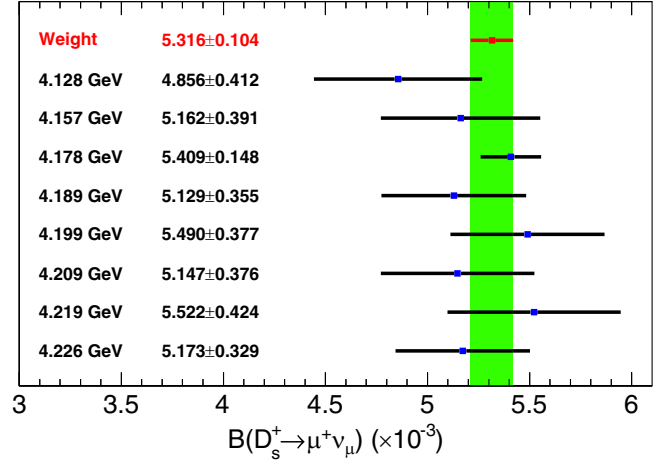


FIG. 4. The obtained BF’s based on individual datasets, where the shown uncertainties are statistical only.

transition $\gamma(\pi^0)$ matched and unmatched are described by individual simulated shapes derived from the signal MC sample, where the former ones are further convolved with a Gaussian function with free parameters to consider the resolution difference between data and MC simulation. The shapes of other backgrounds are derived from the individual MC simulated shapes. In the fit, the BF, the ratios between the signal events with transition $\gamma(\pi^0)$ matched and unmatched, and the background yields are all free.

Figure 3 shows the fit result with all datasets. The BF of $D_s^+ \rightarrow \mu^+\nu_\mu$ is obtained to be

$$\mathcal{B}_{D_s^+ \rightarrow \mu^+\nu_\mu} = (0.5294 \pm 0.0108)\%,$$

which corresponds to a signal yield of 2514.5 ± 51.6 events. Here, the uncertainty is statistical only.

As a cross-check, we measure the BF of $D_s^+ \rightarrow \mu^+\nu_\mu$ based on individual datasets separately, and the obtained results are shown in Fig. 4. The weighted BF of $D_s^+ \rightarrow \mu^+\nu_\mu$, $(0.5316 \pm 0.0104)\%$, is consistent with our nominal result. The different mean values and statistical uncertainties of the BF of $D_s^+ \rightarrow \mu^+\nu_\mu$ are due to slightly different signal and background shapes in different fit strategies, which has been included in the systematic uncertainty of the M_{miss}^2 fit.

VII. SYSTEMATIC UNCERTAINTIES

Sources of the systematic uncertainties in the BF measurement are summarized in Table V. Each of them is estimated relative to the measured BF and described below:

- (i) *ST yield.* The systematic uncertainty is estimated by varying the signal and background shapes in the fit. The alternative signal shapes are obtained by varying the nominal matched angle by $\pm 5^\circ$. The relative difference of the ST yields between data and the

TABLE V. Relative systematic uncertainties in the measurement of the BF of $D_s^+ \rightarrow \mu^+ \nu_\mu$.

Source	Uncertainty (%)
ST yield	0.44
μ^+ tracking	0.24
μ^+ PID	0.19
Transition $\gamma(\pi^0)$ reconstruction	1.00
Least $ \Delta E $ selection	0.70
E_{\max}^{extray} & $N_{\text{ncharged}}^{\text{extra}}$ requirements	0.29
M_{miss}^2 fit	0.72
Quoted BFs	0.34
Contribution from $D_s^+ \rightarrow \gamma \mu^+ \nu_\mu$	0.30
Total	1.61

inclusive MC sample is assigned as the systematic uncertainty. In addition, the uncertainty due to the background fluctuation in the ST yield is also considered as a systematic uncertainty. Adding these three systematic effects quadratically gives a total systematic uncertainty of 0.44%.

- (ii) μ^+ tracking and PID. The μ^+ tracking and PID efficiencies are studied with the control sample $e^+e^- \rightarrow \gamma \mu^+ \mu^-$. After correcting the detection efficiency by $f_{\mu \text{PID}}^{\text{cor}}$, we assign 0.24% and 0.19% as the uncertainties in μ^+ tracking and PID efficiencies, respectively.
- (iii) Transition $\gamma(\pi^0)$ reconstruction. The selection efficiencies of γ and π^0 are studied with $J/\psi \rightarrow \pi^+ \pi^- \pi^0$ decays [51]. The systematic uncertainty is assigned to be 1%.
- (iv) The least $|\Delta E|$ selection. The systematic uncertainty of selecting the transition $\gamma(\pi^0)$ with the least $|\Delta E|$ method is estimated by using the control samples of $D_s^+ \rightarrow K^+ K^- \pi^+$ and $D_s^+ \rightarrow \eta \pi^0 \pi^+$. The difference of the efficiencies of selecting the transition $\gamma(\pi^0)$ candidates between data and MC simulation, 0.70%, is taken as the corresponding systematic uncertainty.
- (v) E_{\max}^{extray} & $N_{\text{ncharged}}^{\text{extra}}$ requirements. The efficiency for the requirements of E_{\max}^{extray} and no extra good charged track is studied with the control samples of $D_s^+ \rightarrow K^+ K^- \pi^+$ and $D_s^+ \rightarrow K_S^0 K^+$. The systematic uncertainty is taken to be 0.29% considering the efficiency differences between data and MC simulation.
- (vi) M_{miss}^2 fit. The systematic uncertainty due to the signal shape with transition $\gamma(\pi^0)$ matched is estimated with an alternative signal shape of a double Gaussian function. The systematic uncertainty due to the signal shape with transition $\gamma(\pi^0)$ unmatched is estimated by replacing the nominal shape with a second-order Chebychev function. The systematic uncertainty due to the real- D_s^- background is estimated by varying the weights of various background

sources within $\pm 1\sigma$ of individual BFs. The systematic uncertainty due to the non- D_s^- background is estimated by varying the shape smoothness parameter from 3 to 2. For different sources, the changes of the fitted signal yield, 0.64%, 0.18%, 0.24%, and 0.10%, are taken as individual uncertainties. The total systematic uncertainty due to the M_{miss}^2 fit is obtained to be 0.72% by adding all four uncertainties in quadrature.

- (vii) Quoted BFs. The uncertainty due to the quoted BFs of D_s^{*-} subdecays from the PDG [47] is examined by varying each subdecay BF by $\pm 1\sigma$. The change of the signal efficiency, 0.34%, is taken as the associated uncertainty.
- (viii) Contribution from $D_s^+ \rightarrow \gamma \mu^+ \nu_\mu$. The systematic uncertainty due to the contribution from the background of $D_s^+ \rightarrow \gamma \mu^+ \nu_\mu$ is estimated with the known upper limit on the BF of $D_s^+ \rightarrow \gamma e^+ \nu_e$ [47]. After fixing this background yield in the M_{miss}^2 fit, the change of the measured BF to the nominal one, 0.30%, is taken as the corresponding systematic uncertainty.

Assuming all systematic uncertainties are independent, the total systematic uncertainty in the measurement of the BF of $D_s^+ \rightarrow \mu^+ \nu_\mu$ is 1.61% by adding them in quadrature. Here, 1.61% corresponds to the absolute systematic uncertainty of 0.0085% for the measured BF.

VIII. RESULTS OF $f_{D_s^+}$ AND $|V_{cs}|$

Combining the measured BF with the world average values of G_F , m_μ , $m_{D_s^+}$, and the D_s^+ lifetime [47] in Eq. (1) yields

$$f_{D_s^+} |V_{cs}| = 241.8 \pm 2.5_{\text{stat}} \pm 2.2_{\text{syst}} \text{ MeV}.$$

Here, the systematic uncertainty arises mainly from the uncertainties in the measured BF (0.8%) and the lifetime of the D_s^+ (0.4%). Taking the CKM matrix element $|V_{cs}| = 0.97349 \pm 0.00016$ from the global SM fit [47] or the averaged decay constant $f_{D_s^+} = 249.9 \pm 0.5 \text{ MeV}$ from recent LQCD calculations [14,17] as input, we determine

$$f_{D_s^+} = 248.4 \pm 2.5_{\text{stat}} \pm 2.2_{\text{syst}} \text{ MeV}$$

and

$$|V_{cs}| = 0.968 \pm 0.010_{\text{stat}} \pm 0.009_{\text{syst}}.$$

The additional systematic uncertainties according to the input parameters are negligible for $|V_{cs}|$ and 0.2% for $f_{D_s^+}$.

Using the BESIII combined result of $\mathcal{B}_{D_s^+ \rightarrow \tau^+ \nu_\tau} = (5.32 \pm 0.07 \pm 0.07)\%$ [13], we obtain $\mathcal{B}_{D_s^+ \rightarrow \tau^+ \nu_\tau} / \mathcal{B}_{D_s^+ \rightarrow \mu^+ \nu_\mu} = 10.05 \pm 0.35$, where the statistical and systematic uncertainties have been combined in quadrature.

TABLE VI. Comparisons between $\mathcal{B}(D_s^+ \rightarrow \mu^+ \nu_\mu)$ and $f_{D_s^+} |V_{cs}|$ measured by various experiments. The first uncertainties are statistical, the second are systematic, and the third are from the input lifetime of D_s^+ . The superscripts a and b denote the measurements are made with and without using the d_{μ^+} requirements.

Experiment	E_{cm} (GeV)	Reaction chain	\mathcal{B} (%)	$f_{D_s^+} V_{cs} $ (MeV)
CLEO [2]	4.170	$e^+ e^- \rightarrow D_s^\pm D_s^{*\mp}$	$0.565 \pm 0.045 \pm 0.017$	$249.8 \pm 10.0 \pm 3.8 \pm 1.0$
BABAR [5]	10.56	$e^+ e^- \rightarrow DKX\gamma D_s^-$	$0.602 \pm 0.038 \pm 0.034$	$257.8 \pm 8.2 \pm 7.3 \pm 1.0$
Belle [6]	10.56	$e^+ e^- \rightarrow DKX\gamma D_s^-$	$0.531 \pm 0.028 \pm 0.020$	$242.2 \pm 6.4 \pm 4.7 \pm 1.0$
BESIII ^b [7]	4.009	$e^+ e^- \rightarrow D_s^+ D_s^-$	$0.517 \pm 0.075 \pm 0.021$	$238.9 \pm 17.5 \pm 4.9 \pm 0.9$
BESIII ^a [8]	4.178	$e^+ e^- \rightarrow D_s^\pm D_s^{*\mp}$	$0.549 \pm 0.016 \pm 0.015$	$246.2 \pm 3.6 \pm 3.4 \pm 1.0$
BESIII ^b [9]	4.178–4.226	$e^+ e^- \rightarrow D_s^\pm D_s^{*\mp}$	$0.535 \pm 0.013 \pm 0.016$	$243.1 \pm 3.0 \pm 3.6 \pm 1.0$
This work^a	4.128–4.226	$e^+ e^- \rightarrow D_s^\pm D_s^{*\mp}$	$0.5294 \pm 0.0108 \pm 0.0085$	$241.8 \pm 2.5 \pm 2.2 \pm 1.0$

This ratio agrees with the SM predicted value of 9.75 within uncertainty, which indicates that no τ - μ LFU violation is observed in the D_s^+ sector.

IX. SUMMARY

In summary, by analyzing 7.33 fb^{-1} of $e^+ e^-$ collision data collected at E_{cm} from 4.128 to 4.226 GeV with the BESIII detector, we measure the $\mathcal{B}(D_s^+ \rightarrow \mu^+ \nu_\mu)$, the product of $f_{D_s^+} |V_{cs}|$, the decay constant $f_{D_s^+}$, and the CKM matrix element $|V_{cs}|$. Comparisons between the $\mathcal{B}(D_s^+ \rightarrow \mu^+ \nu_\mu)$ and $f_{D_s^+} |V_{cs}|$ obtained in this work and the previous measurements are shown in Table VI. These results are important to calibrate various theoretical calculations of $f_{D_s^+}$ and test the unitarity of the CKM matrix with better accuracy. We also test LFU with $D_s^+ \rightarrow \ell^+ \nu_\ell$ decays, and no τ - μ LFU violation is found.

ACKNOWLEDGMENTS

The BESIII Collaboration thanks the staff of BEPCII and the IHEP computing center for their strong support. This work is supported in part by National Key R&D Program of China under Contracts No. 2020YFA0406400 and No. 2020YFA0406300; National Natural Science Foundation of China (NSFC) under Contracts No. 11875170, No. 12035009, No. 11635010, No. 11735014, No. 11835012, No. 11935015, No. 11935016, No. 11935018, No. 11961141012, No. 12022510, No. 12025502, No. 12035013, No. 12061131003, No. 12192260, No. 12192261,

No. 12192262, No. 12192263, No. 12192264, No. 12192265, No. 12221005, No. 12225509, and No. 12235017; the Chinese Academy of Sciences (CAS) Large-Scale Scientific Facility Program; the CAS Center for Excellence in Particle Physics (CCEPP); CAS Key Research Program of Frontier Sciences under Contracts No. QYZDJ-SSW-SLH003 and No. QYZDJ-SSW-SLH040; 100 Talents Program of CAS; The Institute of Nuclear and Particle Physics (INPAC) and Shanghai Key Laboratory for Particle Physics and Cosmology; ERC under Contract No. 758462; European Union's Horizon 2020 research and innovation programme under Marie Skłodowska-Curie grant agreement under Contract No. 894790; German Research Foundation DFG under Contracts No. 443159800 and No. 455635585, Collaborative Research Center Grants No. CRC 1044, No. FOR5327, and No. GRK 2149; Istituto Nazionale di Fisica Nucleare, Italy; Ministry of Development of Turkey under Contract No. DPT2006K-120470; National Research Foundation of Korea under Contract No. NRF-2022R1A2C1092335; National Science and Technology fund of Mongolia; National Science Research and Innovation Fund (NSRF) via the Program Management Unit for Human Resources & Institutional Development, Research and Innovation of Thailand under Contract No. B16F640076; Polish National Science Centre under Contract No. 2019/35/O/ST2/02907; The Swedish Research Council; and U.S. Department of Energy under Contract No. DE-FG02-05ER41374.

- [1] D. Silverman and H. Yao, *Phys. Rev. D* **38**, 214 (1988).
 [2] J. P. Alexander *et al.* (CLEO Collaboration), *Phys. Rev. D* **79**, 052001 (2009).
 [3] P. Naik *et al.* (CLEO Collaboration), *Phys. Rev. D* **80**, 112004 (2009).

- [4] P. U. E. Onyisi *et al.* (CLEO Collaboration), *Phys. Rev. D* **79**, 052002 (2009).
 [5] P. del Amo Sanchez *et al.* (BABAR Collaboration), *Phys. Rev. D* **82**, 091103 (2010); **91**, 019901(E) (2015).

- [6] A. Zupanc *et al.* (Belle Collaboration), *J. High Energy Phys.* **09** (2013) 139.
- [7] M. Ablikim *et al.* (BESIII Collaboration), *Phys. Rev. D* **94**, 072004 (2016).
- [8] M. Ablikim *et al.* (BESIII Collaboration), *Phys. Rev. Lett.* **122**, 071802 (2019).
- [9] M. Ablikim *et al.* (BESIII Collaboration), *Phys. Rev. D* **104**, 052009 (2021).
- [10] M. Ablikim *et al.* (BESIII Collaboration), *Phys. Rev. D* **104**, 032001 (2021).
- [11] M. Ablikim *et al.* (BESIII Collaboration), *Phys. Rev. Lett.* **127**, 171801 (2021).
- [12] M. Ablikim *et al.* (BESIII Collaboration), *J. High Energy Phys.* **09** (2023) 124.
- [13] M. Ablikim *et al.* (BESIII Collaboration), [arXiv:2303.12600](https://arxiv.org/abs/2303.12600).
- [14] A. Bazavov *et al.*, *Phys. Rev. D* **98**, 074512 (2018).
- [15] B.-C. Ke, J. Koponen, H.-B. Li, and Y. Zheng, *Annu. Rev. Nucl. Part. Sci.* **73**, 285 (2023).
- [16] A. Bazavov *et al.* (Fermilab Lattice and MILC Collaborations), *Phys. Rev. D* **90**, 074509 (2014).
- [17] N. Carrasco *et al.*, *Phys. Rev. D* **91**, 054507 (2015).
- [18] P. A. Boyle, L. Del Debbio, A. Jüttner, A. Khamseh, F. Sanfilippo, and J. T. Tsang, *J. High Energy Phys.* **12** (2017) 008.
- [19] A. Bazavov *et al.* (Fermilab Lattice and MILC Collaborations), *Phys. Rev. D* **85**, 114506 (2012).
- [20] C. T. H. Davies, C. McNeile, E. Follana, G. P. Lepage, H. Na, and J. Shigemitsu, *Phys. Rev. D* **82**, 114504 (2010).
- [21] H. Na, C. T. H. Davies, E. Follana, G. P. Lepage, and J. Shigemitsu, *Phys. Rev. D* **86**, 054510 (2012).
- [22] P. Dimopoulos *et al.* (ETM Collaboration), *J. High Energy Phys.* **01** (2012) 046.
- [23] W.-P. Chen, Y.-C. Chen, T.-W. Chiu, H.-Y. Chou, T.-S. Guu, and T.-H. Hsieh (TWQCD Collaboration), *Phys. Lett. B* **736**, 231 (2014).
- [24] Y. Namekawa *et al.* (PACS-CS Collaboration), *Phys. Rev. D* **84**, 074505 (2011).
- [25] D. Becirevic, B. Blossier, A. Gerardin, A. Le Yaouanc, and F. Sanfilippo, *Nucl. Phys.* **B872**, 313 (2013).
- [26] J. P. Lees *et al.* (BABAR Collaboration), *Phys. Rev. Lett.* **109**, 101802 (2012).
- [27] J. P. Lees *et al.* (BABAR Collaboration), *Phys. Rev. D* **88**, 072012 (2013).
- [28] R. Aaij *et al.* (LHCb Collaboration), *Phys. Rev. Lett.* **115**, 111803 (2015); **115**, 159901(E) (2015).
- [29] R. Aaij *et al.* (LHCb Collaboration), *Phys. Rev. Lett.* **120**, 171802 (2018).
- [30] R. Aaij *et al.* (LHCb Collaboration), *Phys. Rev. D* **97**, 072013 (2018).
- [31] G. Aad *et al.* (ATLAS Collaboration), *Phys. Rev. D* **92**, 072004 (2015).
- [32] G. Caria *et al.* (Belle Collaboration), *Phys. Rev. Lett.* **124**, 161803 (2020).
- [33] S. Hirose *et al.* (Belle Collaboration), *Phys. Rev. Lett.* **118**, 211801 (2017).
- [34] Y. S. Amhis *et al.* (Heavy Flavor Averaging Group, HFLAV Collaboration), *Phys. Rev. D* **107**, 052008 (2023).
- [35] M. Ablikim *et al.* (BESIII Collaboration), *Nucl. Instrum. Methods Phys. Res., Sect. A* **614**, 345 (2010).
- [36] C. Yu *et al.*, in *7th International Particle Accelerator Conference* (JACoW, Geneva, Switzerland, 2016), pp. 1014–1018.
- [37] X. Li *et al.*, *Radiat. Detect. Technol. Methods* **1**, 12 (2022).
- [38] Y. Guo *et al.*, *Radiat. Detect. Technol. Methods* **1**, 14 (2017).
- [39] M. Ablikim *et al.* (BESIII Collaboration), *Chin. Phys. C* **39**, 093001 (2015).
- [40] M. Ablikim *et al.* (BESIII Collaboration), *Chin. Phys. C* **46**, 113002 (2022).
- [41] S. Agostinelli *et al.* (GEANT4 Collaboration), *Nucl. Instrum. Methods Phys. Res., Sect. A* **506**, 250 (2003).
- [42] S. Jadach, B. F. L. Ward, and Z. Was, *Comput. Phys. Commun.* **130**, 260 (2000).
- [43] S. Jadach, B. F. L. Ward, and Z. Was, *Phys. Rev. D* **63**, 113009 (2001).
- [44] R.-G. Ping, *Chin. Phys. C* **38**, 083001 (2014).
- [45] D. J. Lange, *Nucl. Instrum. Methods Phys. Res., Sect. A* **462**, 152 (2001).
- [46] R.-G. Ping, *Chin. Phys. C* **32**, 599 (2008).
- [47] R. Workman *et al.* (Particle Data Group Collaboration), *Prog. Theor. Exp. Phys.* **2022**, 083C01 (2022).
- [48] J. C. Chen, G. S. Huang, X. R. Qi, D. H. Zhang, and Y. S. Zhu, *Phys. Rev. D* **62**, 034003 (2000).
- [49] R.-L. Yang, R.-G. Ping, and H. Chen, *Chin. Phys. Lett.* **31**, 061301 (2014).
- [50] E. Richter-Was, *Phys. Lett. B* **303**, 163 (1993).
- [51] M. Ablikim *et al.* (BESIII Collaboration), *Phys. Rev. D* **83**, 112005 (2011).